Lasers in Manufacturing Conference 2021

Cavitation phenomena in BA-LIFT

Juan José Moreno Labella[1,2], Miguel Morales Furió[1,2], David Muñoz Martín[1,3], Carlos Molpeceres Álvarez[1,2]

[1]*Centro Láser, Universidad Politécnica de Madrid, Spain*
[2]*Escuela Técnica Superior de Ingenieros Industriales, Universidad Politécnica de Madrid, Spain*
[3]*Escuela Técnica Superior de Ingeniería y Diseño Industrial, Universidad Politécnica de Madrid, Spain*

Abstract

In Blister-Actuated Laser-Induced Forward Transfer (BA-LIFT) the direct interaction between the laser pulse and the transference fluid is removed interposing an intermediate polyimide layer that absorbs and pushes away the fluid. A study of the transference mechanisms has been made through a Phase Field model in COMSOL Multiphysics. The differences between the experimental images and the simulations led to the suggestion of a cavitation bubble. Contrary to the LIFT process, this bubble cannot be laser-induced, as there is no direct interaction owing to the polyimide layer, so it must be mechanically induced.

In this work, some shadowgraphy images of the cavitation bubble along with its effects on the Phase Field FEM-CFD model are shown. In the numerical model, the expansion of the main jet –including the observed secondary effects– can be reproduced. Including a second push 9 μs after the blister expansion makes the fluid take the secondary effects' shapes. Considering a cavitation bubble like in other LIFT processes –in which the bubble has been generated directly by the laser pulse–, there are three possible causes of its appearance: absorption of the laser pulse in the fluid –through the polyimide intermediate layer–, thermal evaporation due to heat conduction, or pressure fall due to fluid velocity. Besides, a mechanical rebound of the elastically deformed blister has also been considered, as the effects in the model suggest. After the analysis, the only explanations that cannot be rejected –the depressurization area in front of the blister– led to the proposed hypothesis: the velocity field from the blister expansion causes a cavitation bubble in front of itself, whose effects are equivalent to the cavitation of the vapor bubble described in other LIFT techniques.

Keywords: Laser-Induced Forward Transfer (LIFT); Blister-Assisted Laser-Induced Forward Transfer (BA-LIFT); Laser process modeling; Fluid dynamics;

* Corresponding author.
E-mail address: juanjose.moreno.labella@upm.es .

1. Introduction

Blister-Actuated Laser-Induced Forward Transfer (BA-LIFT) is a modified LIFT process to transfer small volumes of fluid without interaction with the laser pulse. To achieve that, an intermediate polymeric layer is set in the laser beam path between the glass substrate and the fluid (Brown, Kattamis, & Arnold, 2010; Márquez et al., 2020). Some unexpected effects during the formation of the jet such as bulgy shapes have been spotted (Moreno-Labella, Munoz-Martin, Márquez, Morales, & Molpeceres, 2021), though they cannot be explained only considering the flow dynamics derived from a pure mechanical push. The observed dynamics fit with the appearance of a cavitation bubble, which has been observed, and whose effects have been introduced in the CFD-FEM model to replicate the effects. The images have been acquired using a high-speed time-resolved shadowgraphy system (Moreno-Labella et al., 2021).

2. Laminar-Flow Phase-Field FEM-CFD model

A FEM CFD axisymmetric model has been built in COMSOL Multiphysics® 5.3a to simulate the BA-LIFT process. The Phase-Field method, which considers the minimization of mixing energy taken as the sum of the surface energy and bulk energy of the flow (Yue, Feng, Liu, & Shen, 2004), has been chosen for this study instead of Level Set (López, 2017; Rubio, 2014) or Volume of Fluid definitions (VOF) (Brasz, Arnold, Stone, & Lister, 2015; Kalaitzis et al., 2019). The Phase-Field auxiliary function to follow the interface, Φ, has a range of values between 0 (fluid) to 1 (air) –the interface, thus, is diffuse and centered around 0.5–, according to the definition of the method in COMSOL Multiphysics® (COMSOL multiphysics® [computer software]).

The motion of each phase is governed by two fluid mechanics equations (Batchelor, 2007; Ferziger, Peric, & Street, 2019; Gresho & Sani, 2000; Panton, 2005): continuity equation particularized for incompressible flow (1) and momentum equation (2), both from Navier-Stokes equations.

$$\nabla \cdot \mathrm{u} = 0 \tag{1}$$

$$\rho\, \partial \mathrm{u}/\partial \mathrm{t} + \rho(\mathrm{u} \cdot \nabla)\mathrm{u} = \nabla \cdot [-\mathrm{pI} + \mu(\nabla \mathrm{u} + \nabla \mathrm{u}^{\mathrm{T}})] + \mathrm{F_g} + \mathrm{F_{st}} \tag{2}$$

The last two terms in equation (2) are two external forces: gravity ($\mathrm{F_g}$) and surface tension ($\mathrm{F_{st}}$). In the model, $\mathrm{F_g}$ has so little influence that it can be neglected, so only surface tension remains present in (2), and is implemented in Phase-Field method as follows, involving G, the chemical potential (Yue et al., 2004):

$$\mathrm{F_{st}} = \mathrm{G}\nabla\phi \tag{3}$$

$$\mathrm{G} = \lambda(-\nabla^2\phi + \phi(\phi^2 - 1)/\varepsilon^2) \tag{4}$$

In these equations, λ stands for the mixing energy density, and ε represents a capillary width linked to the thickness of the fluid interface. There are two additional equations to track the position of the interface:

$$\partial\phi/\partial \mathrm{t} + (\mathrm{u} \cdot \nabla)\phi = \nabla \cdot \gamma\lambda/\varepsilon^2\, \nabla\psi \tag{5}$$

$$\psi = -\nabla \cdot \varepsilon^2\nabla\phi + (\phi^2 - 1)\phi \tag{6}$$

These involved quantities, as well as γ and σ –the surface tension coefficient– are interrelated through:

$$\sigma = 2\sqrt{2}/3 \cdot \lambda/\varepsilon \tag{7}$$

$$\gamma = \chi\varepsilon^2 \tag{8}$$

The mobility tuning parameter, χ, governs the diffusion-related time for the interface, according to the Cahn-Hilliard diffusion (Cahn & Hilliard, 1958). The volume fraction of fluid is computed as follows:

$$V_f = \min(\max((1+\phi)/2, 0), 1) \tag{9}$$

The properties of the materials are calculated as the weighted sum of those of each phase:

$$\rho = V_f\rho_2 + (1 - V_f)\rho_1 \tag{10}$$

$$\mu = V_f\mu_2 + (1 - V_f)\mu_1 \tag{11}$$

The movement of the fluid in BA-LIFT is only induced by the push of the blister, implemented as a moving wall. This blister model, shown in equations (12-16), has been similarly set in some other studies (Brown, 2011; López, 2017; Rubio, 2014). The blister has been estimated by taking images and measuring it for the work conditions using a high-speed imaging system. Its evolution may be split into two separable functions: its spatial evolution, only dependent on its radius –B(r)–, and its unitary time response –T(t)–. By multiplying these two functions, the displacement equation turns out as follows:

$$\delta(r, t) = B(r) \cdot T(t) \tag{12}$$

To define T(t), many images of the blister expansion have been taken to fix the parameters of the polynomial steps. This experiment was done at 22 µJ, a typical work energy value (Fig. 1). Three stages are distinguished: an initial quick expansion, an elastic shrinking recovery, and a stabilized stage. In the model, the blister expands for the first 70 ns. Then, it recovers elastically within the following 0.5 µs. Once it has deflated, it is assumed that no further evolution takes place.

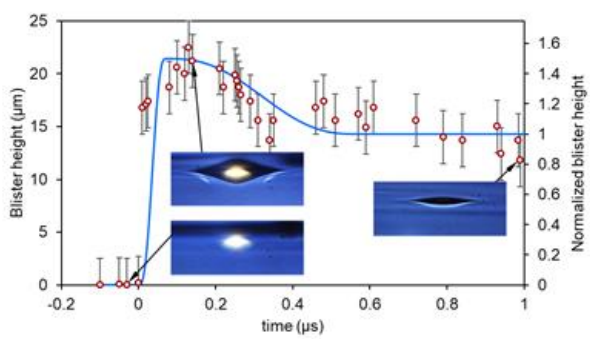

Fig. 1. First-microsecond analysis and modeling of blister dynamics for 22 µJ. Blister height measurements (red circles) are plotted in real height units and polynomial fit (blue solid line) is represented as a normalized height by dividing by the infinite-time blister height. Representative images have also been put along to exemplify the three different stages during blister evolution (Moreno-Labella et al., 2021)

Height data –and thus the temporal function– has been normalized by dividing the measurements between the blister infinite-time height –after a microsecond–. The resultant curve is the input for the model (Fig. 1 and Fig. 4), written –with time in microseconds– as the linear combination of two unitary steps:

$$T_1(t) = 3569941 \cdot t^5 - 624740 \cdot t^4 + 29155 \cdot t^3 \tag{13}$$

$$T_2(t) = -192 \cdot t^5 + 240 \cdot t^4 - 80 \cdot t^3 \tag{14}$$

$$T(t) = \begin{cases} 1.5 \cdot T_1(t) & t < 0.070\ \mu s \\ 1.5 + 0.5 \cdot T_2(t - 0.07) & 0.070\ \mu s \leq t < 0.570\ \mu s \\ 1 & t \geq 0.570\ \mu s \end{cases} \quad (15)$$

The spatial function takes acquaintance of the geometrical shape of the blister (Fig. 2) –without taking into account its time evolution– by the mathematical function:

$$B(r) = H_0\left(\max((1 - r/R_0)^2, 0)\right)^{1.25} \quad (16)$$

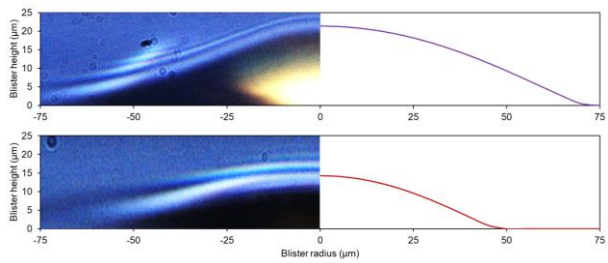

Fig. 2. Blister shape function and blister image comparison at its maximum (up) and at a stabilized time (down). The laser pulse is still visible in the first image (Moreno-Labella et al., 2021)

H_0 and R_0 are the height and the radius of the blister, respectively, at times at which no significant evolution occurs. Their dependence on the energy is given by a second-degree polynomial for the height and logarithmic function for the radius (Hong, 2020). Sweeping over the energy from 15 to 50 µJ allows fitting the proposed curves for these work conditions (Fig. 3).

$$H_0 = -0.0006 \cdot E^2 + 0.3421 \cdot E + 7.0237 \quad (17)$$

$$R_0 = 9 \cdot \log(E) + 20 \quad (18)$$

In these equations (Equations 17 and 18), E stands for the laser pulse energy. Some examples of these images are shown in Fig. 1 and Fig. 2.

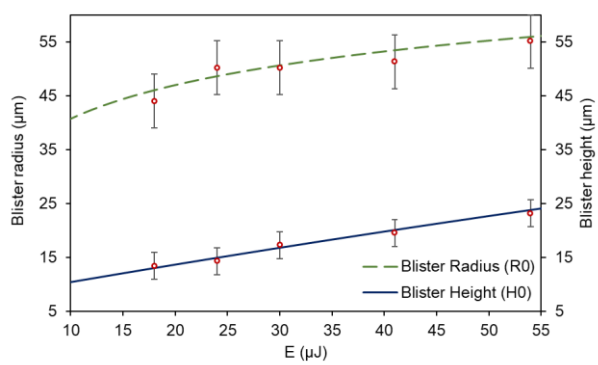

Fig. 3. Polynomial and logarithmic adjustment for blister height (blue-solid line) and radius (green-dash line), respectively, for times at which no further quick evolution has been observed in the blister, as a function of laser pulse energy. Experimental points have been added over its corresponding line (Moreno-Labella et al., 2021)

This parametrization simplifies the model, as only E is needed to define the blister dimensions. The described model closely replicates BA-LIFT for typical transferences. Different conditions have been simulated and validated both against other published models and images taken by the described system (Brown, Brasz, Ventikos, & Arnold, 2012).

3. Simulations of BA-LIFT standard regimes

Under ideal conditions, the BA-LIFT transference occurs through a single laminar jet (Yan, Huang, Xu, & Chrisey, 2012). This transference regime is closely replicated by the described model (Fig. 6). The temporal evolution of the blister (Fig. 4) is derived from image studies carried out by some authors (Brown et al., 2010; Kattamis, Brown, & Arnold, 2011) and blister measurements obtained with the time-resolved image acquisition system (Fig. 1 and Fig. 2).

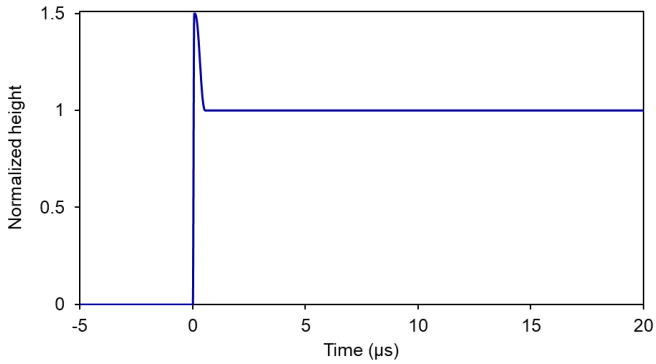

Fig. 4. Temporal function of the blister for the first 20 µs with no consideration of further effects (Moreno-Labella et al., 2021)

The non-transference regime –in which the fluid is only elastically deformed– appears for low laser pulse energies, high viscosities, or thick layers of fluid. Experimental images and simulation results are compared in Fig. 5 for a particular case of this regime of transference for high viscosity water-glycerol mixture (80 %wt glycerol; 45 mPa·s (Cheng, 2008)). The experimental fluid layer thickness is set to 70±10 µm. In the model, the best agreement with the experiments was obtained for 60 µm fluid thickness considering a laser pulse energy of 19 µJ.

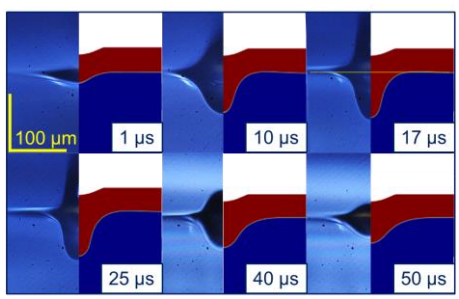

Fig. 5. Non-transference regime images versus simulation comparison (fluid: water-glycerol at 80 %wt, 45 mPa·s, thickness: 70±10 µm (experimental) and 60 µm (simulation), energy: 19 µJ) (Moreno-Labella et al., 2021)

On the contrary, the jet-transference regime occurs for high laser pulse energies, low viscosities, or thin layers of fluid. The starting fluid bell-like structure has enough energy to beat surface tension and viscosity forces and travels towards the acceptor as a jet. Experimental images and simulation results are compared in

Fig. 6 for a particular case of this regime of transference for intermediate viscosity water-glycerol mixture (66 %wt glycerol; 13 mPa·s (Cheng, 2008)). Fluid layer thickness is set to 30±10 µm. In the model, the best agreement with the experiments has been obtained for 40 µm thickness considering a laser pulse energy of 27 µJ.

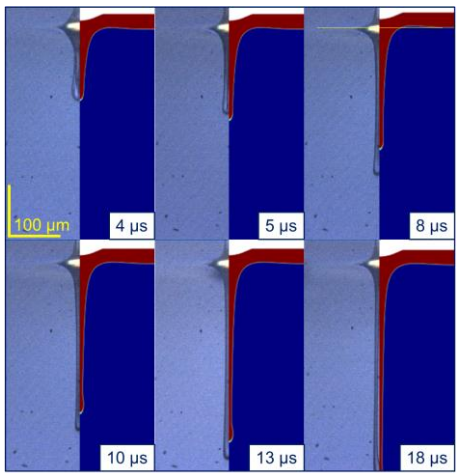

Fig. 6. Jet regime images versus simulation comparison (fluid: water-glycerol at 66 %wt, 13 mPa·s, thickness: 30±10 µm (experimental) and 40 µm (simulation), energy: 27 µJ) (Moreno-Labella et al., 2021)

4. Cavitation bubble images: a modified BA-LIFT setup

The standard BA-LIFT setup was modified to study the appearance of a bubble in front of the polyimide layer. To this purpose, a BA-LIFT substrate –glass and polyimide layer– was placed onto a mass of pure water confined in an optical glass cuvette instead of a thin layer (Fig. 7) to avoid the distortion of the interface in the optical path of the camera. The acquired images have been taken through the same high-speed image system as in the standard regimes study for water-glycerol mixtures (Moreno-Labella et al., 2021). Though no jet is generated due to the fluid confinement, and thus the fluid speeds are lower than in regular BA-LIFT, the fluid used in this experiment –pure water– is easier to suffer from cavitation due to its lower viscosity and vapor pressure (Carr, Townsend, & Badger, 1925).

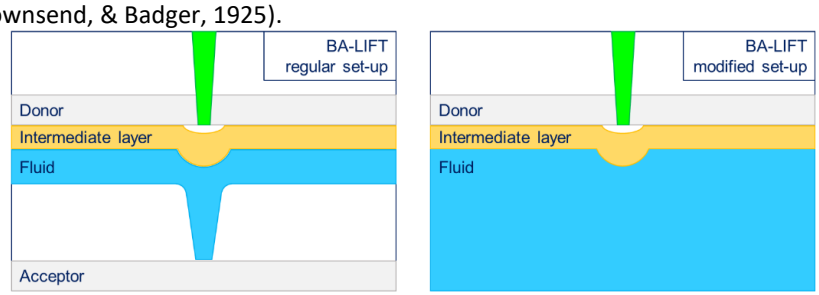

Fig. 7. Regular setup for BA-LIFT (left): a thin layer of fluid ejects a small portion of the material, and modified setup (right): an infinite mass of fluid is set below the polyimide layer for this study (Moreno-Labella, Munoz-Martin, Morales, & Molpeceres, 2021)

In the acquired images, the spot in which the laser pulse interacts with the polyimide layer can be seen. An infinite-time image is shown to spot the shape and size of the stabilized-time blister, as a reference (Fig. 8, d). For short times (less than 9 µs), either a single or multiples cavitation bubbles grow and join (Fig. 8, a) until it overexpands at its maximum (Fig. 8, b). Then, it starts to contract until its implosion (Fig. 8, c), whose dynamics follow the behavior of cavitation bubbles generated by direct laser interaction or high-frequency sonic waves, for instance (Maiga, 2016). The described model (Moreno-Labella et al., 2021) was also used to analyze the pressure field generated in this modified setup, whose results at 1 µs are shown in Fig. 8, e. As no phase change has been included in the model, it only shows the possibility of cavitation phenomena without considering the dynamics of the bubble. The behavior of the bubble varies in time due to the specific conditions of each single laser pulse, but its implosion always happens between 7 and 11 µs.

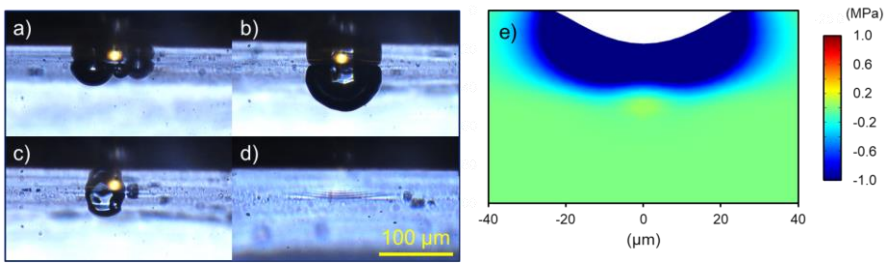

Fig. 8. Directly-observed bubble below the polyimide layer at short times (less than 9 µs) (a), at its maximum expansion (around 9 µs) (b), and its contraction stage (after 9 µs) (c). A long-time image shows the blister without the bubble (d), as well as the depressurized zone at 1 µs in the described CFD model (e) (Moreno-Labella et al., 2021)

5. Model modification to include the effects of the cavitation bubble

The fluid is accelerated after the implosion of the cavitation bubble, so a second push is introduced *ad hoc* in the model moving wall, similarly as the first initial movement reproduces the expansion of the blister (Fig. 9). The adjustment of the delay (τ) between the two pushes has been made through the analysis of the experimental images. The best results are gotten when the second push happens at times near 9 µs. The temporal function is defined in Equation 19.

$$T(t) = \begin{cases} 1.5 \cdot T_1(t) & t < 0.070\ \mu s \\ 1.5 + 0.5 \cdot T_2(t - 0.07) & 0.070\ \mu s \leq t < 0.120\ \mu s \\ 1 & 0.120\ \mu s \leq t < 8.500\ \mu s \\ 1 + T_2(t - 8.5) & 8.500\ \mu s \leq t < 9.000\ \mu s \\ 1.5 \cdot T_1(t - 9.0) & 9.000\ \mu s \leq t < 9.070\ \mu s \\ 0.5 \cdot T_2(t - 9.07) & 9.070\ \mu s \leq t < 9.570\ \mu s \\ 1 & t \geq 9.570\ \mu s \end{cases} \quad (19)$$

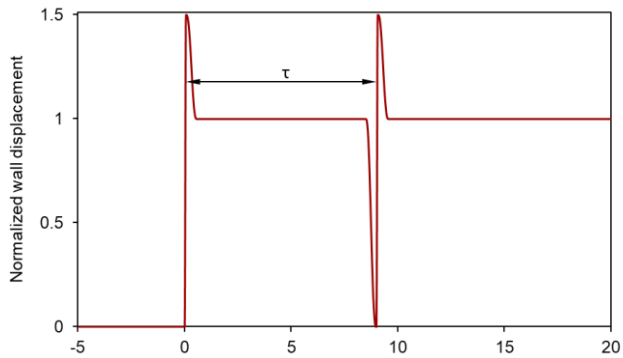

Fig. 9. The modified temporal function that includes the blister push and the second push due to the bubble at 9 µs (Moreno-Labella et al., 2021)

This simplified model closely reproduces the bulgy shapes by only introducing this second push, as shown in Fig. 10. The fluid is water-glycerol at 66 %wt (13 mPa·s), in a layer of 30±10 µm thick in the experiments and 40 µm in the simulation, with a pulse energy of 48 µJ. In the first row, the second image (Fig. 10, 0.5 µs) compares the initial growth of the deformed shape: simulation and experiments are close. The third comparison in the series (Fig. 10, 3.0 µs) shows that the experimental image differs from the simulation as said before. The fluid develops in a much wider bell-like shape, possibly because a phase change occurs, an amount of vapor is generated, and expands itself (Robinson, Blake, Kodama, Shima, & Tomita, 2001). After a while (Fig. 10, 7.0 µs, and 9.0 µs), the over-expanded bell begins to collapse, and the simulation and the experiments come close again. In the second row, the push of the fluid takes place. The first image (Fig. 10, 9.0 µs) shows the time at which the jet has the shape that the only mechanical model predicts. After the second push in the simulation and the pressure peak in the experiment, a bulgy shape begins to grow in the shape of small shoulders, as compared in the next two pictures (Fig. 10, 10.0 µs and 12.0 µs). Finally, surface tension reshapes the modified jet and fluid detachment is seen in both experiments and simulation (Fig. 10, 14.0 µs). Only including the push that has been observed in the images is enough to replicate the secondary effects.

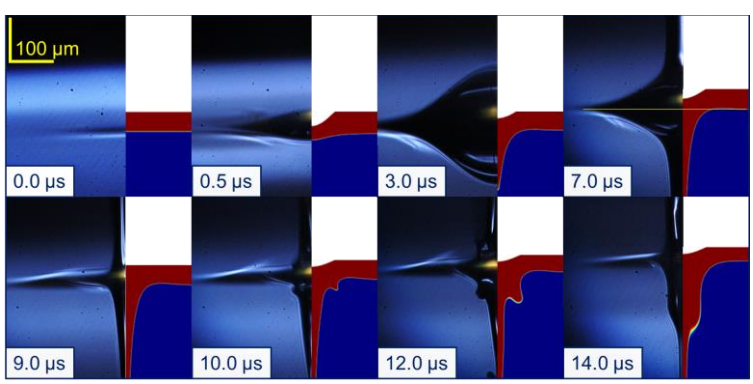

Fig. 10. Comparison between acquired images and simulations considering water-glycerol mixture. Secondary effects are closely simulated assuming the second push. Two stages can be distinguished: bubble generation phase (upper row) and bubble burst phase (lower row) (fluid: water-glycerol at 66 %wt, 13 mPa·s, thickness: 30±10 µm (experimental) and 40 µm (simulation), energy: 48 µJ) (Moreno-Labella et al., 2021)

6. Conclusions

Shadowgraphy images of the jet generated in BA-LIFT have been compared to simulations in COMSOL. The transference regimes, such as jet expansion or bulgy shapes, that have been previously observed in other LIFT techniques, have been also experimentally obtained by introducing the effects of an observed cavitation bubble as an *ad hoc* second push of the moving wall at 9 µs from the expansion of the blister.

The BA-LIFT process has been characterized due to the absence of direct interaction between the laser pulse and the fluid, so it is an only and purely mechanical process. The bubble must come from the depressurization of the fluid in front of the blister, given the impossibility of laser absorption in the fluid. Besides, several images of the cavitation bubble have been acquired considering an infinite fluid setup instead of a thin layer. Its appearance and implosion match the shape that the BA-LIFT jet gets for short times –explained by the purely mechanical model–, as well as the come-up of the bulgy shapes for intermediate times –only after considering the presence of a cavitation bubble–.

Acknowledgments

This research has been funded by the Spanish MINECO project SCALED (PID2019-109215RB-C44), and Comunidad de Madrid Projects ADITIMAT-CM (S2018/NMT-4411), and BIOPIELTEC-CM (P2018/BAA4480).

References

Batchelor, G. K. (2007). *An introduction to fluid dynamics* (9th ed.). Cambridge: Cambridge Univ. Press.

Brasz, F. C., Arnold, C. B., Stone, H. A., & Lister, J. R. (2015). Early-time free-surface flow driven by a deforming boundary. *Journal of Fluid Mechanics, 767*, 811-841. doi:10.1017/jfm.2015.74

Brown, M. S. (2011). *Experimental and numerical study of laser-induced forward transfer printing of liquids* Available from Dissertations & Theses Europe Full Text: Science & Technology. Retrieved from http://www.riss.kr/pdu/ddodLink.do?id=T12877065

Brown, M. S., Brasz, F. C., Ventikos, Y., & Arnold, C. B. (2012). Impulsively actuated jets from thin liquid films for high-resolution printing applications. *Journal of Fluid Mechanics, 709*, 341. doi:10.1017/jfm.2012.337

Brown, M. S., Kattamis, N., & Arnold, C. B. (2010). Time-resolved study of polyimide absorption layers for blister-actuated laser-induced forward transfer. *Journal of Applied Physics, 107*(8), 083103-8. doi:10.1063/1.3327432

Cahn, J. W., & Hilliard, J. E. (1958). Free energy of a nonuniform system. I. interfacial free energy. *The Journal of Chemical Physics, 28*(2), 258-267. doi:10.1063/1.1744102

Carr, A. R., Townsend, R. E., & Badger, W. L. (1925). Vapor pressures of glycerol-water and glycerol-water-sodium chloride systems. *Industrial & Engineering Chemistry, 17*(6), 643-646. doi:10.1021/ie50186a043

Cheng, N. (2008). Formula for the viscosity of a glycerol-water mixture. *Industrial and Engineering Chemistry Research, 47*(9), 3285-3288. doi:10.1021/ie071349z

COMSOL multiphysics® [computer software]. Stockholm, Sweden: COMSOL AB.

Ferziger, J. H., Peric, M., & Street, R. L. (2019). *Computational methods for fluid dynamics* (4th ed.). Switzerland: Springer International Publishing.

Gresho, P. M., & Sani, R. L. (2000). *Incompressible flow and the finite element method*. Chichester: Wiley.

Hong, J. (2020). Thermo-mechanical analysis of blister formation on a rigid substrate in blister-actuated laser-induced forward transfer. *IEEE Transactions on Components, Packaging and Manufacturing Technology, 10*(4), 637-643. doi:10.1109/TCPMT.2019.2959708

Kalaitzis, A., Makrygianni, M., Theodorakos, I., Hatziapostolou, A., Melamed, S., Kabla, A., . . . Zergioti, I. (2019). Jetting dynamics of newtonian and non-newtonian fluids via laser-induced forward transfer: Experimental and simulation studies. *Applied Surface Science, 465*, 136-142. doi:10.1016/j.apsusc.2018.09.084

Kattamis, N. T., Brown, M. S., & Arnold, C. B. (2011). Finite element analysis of blister formation in laser-induced forward transfer. *Journal of Materials Research, 26*(18), 2438-2449. doi:10.1557/jmr.2011.215

López, I. (2017). *Simulación de procesos de transferencia de material con láser asistida por capa de polímero (BA-LIFT)*

Maiga, M. A. (2016). Particle model of single bubble sonoluminescence. *International Journal of Physical Sciences, 11*(19), 252-261. doi:10.5897/IJPS2016.4535

Márquez, A., Gómez-Fontela, M., Lauzurica, S., Candorcio-Simón, R., Muñoz-Martín, D., Morales, M., . . . Molpeceres, C. (2020). Fluorescence enhanced BA-LIFT for single cell detection and isolation. *Biofabrication, 12*(2), 025019. doi:10.1088/1758-5090/ab6138

Moreno-Labella, J. J., Munoz-Martin, D., Márquez, A., Morales, M., & Molpeceres, C. (2021). Numerical study of water-glycerol BA-LIFT: Analysis and simulation of secondary effects. *Optics & Laser Technology, 135* doi:10.1016/j.optlastec.2020.106695

Moreno-Labella, J. J., Munoz-Martin, D., Morales, M., & Molpeceres, C. (2021). Cavitation bubble evidence in BA-LIFT processes. *Results in Physics, 103955* doi:10.1016/j.rinp.2021.103955

Panton, R. L. (2005). *Incompressible flow* (3rd ed.). New York: Wiley.

Robinson, P. B., Blake, J. R., Kodama, T., Shima, A., & Tomita, Y. (2001). Interaction of cavitation bubbles with a free surface. *Journal of Applied Physics, 89*(12), 8225-8237. doi:10.1063/1.1368163

Rubio, L. (2014). *Simulación con COMSOL de procesos de transferencia de material inducida por láser*

Yan, J., Huang, Y., Xu, C., & Chrisey, D. B. (2012). Effects of fluid properties and laser fluence on jet formation during laser direct writing of glycerol solution. *Journal of Applied Physics, 112*(8), 83105. doi:10.1063/1.4759344

Yue, P., Feng, J. J., Liu, C., & Shen, J. (2004). A diffuse-interface method for simulating two-phase flows of complex fluids. *Journal of Fluid Mechanics, 515*, 293-317. doi:10.1017/S0022112004000370